Nuclear Instruments and Methods in Physics Research B 355 (2015) 369–373

Contents lists available at ScienceDirect

Nuclear Instruments and Methods in Physics Research B

journal homepage: www.elsevier.com/locate/nimb

Measurements of coherent interactions of 400 GeV protons in silicon bent crystals

Roberto Rossi [a,b,*], Gianluca Cavoto [b], Daniele Mirarchi [a], Stefano Redaelli [a], Walter Scandale [a]

[a] CERN, European Organization for Nuclear Research, CH-1211 Geneva 23, Switzerland
[b] INFN Sezione di Roma, Piazzale Aldo Moro 2, 00185 Rome, Italy

ARTICLE INFO

Article history:
Received 14 December 2014
Received in revised form 1 March 2015
Accepted 1 March 2015
Available online 16 March 2015

Keywords:
LHC
Collimation
Crystal
Protons
UA9

ABSTRACT

Within UA9 Collaboration bent silicon crystals has been irradiated by 400 GeV proton beams at the H8 line of the CERN SPS North Area. Proton–crystal interactions were investigated by analyzing the particle trajectories hitting the crystal. 26 crystals were tested and 10 of them used to extract key crystal properties, such as bending angle, channeling efficiency and so on. A statistical analysis of the results is presented. The results provide experimental data to be used for an exhaustive comparison with simulation routines.

1. Introduction

Crystal channeling [1–3] can be used to develop a collimation system based on bent crystals for high intensity machines like the Large Hadron Collider (LHC). A first step towards the studies for LHC application [4] is the experimental characterization of bent crystals with high-energy proton beams. The crystals are tested at the SPS H8 extraction line to study the interaction with 400 GeV protons. The H8 tests are used to study single pass interactions, and then complemented by the tests with circulating beams at SPS, with protons and ions at the energies of 120 and 270 GeV [5–8].

In addition to the characterization of the crystals, beam tests are also providing crucial input for simulation tools. In particular, single pass data from H8 have been used to evaluate the predictivity of simulation routines [9,10]. Examples of this comparison are presented in [11–13]. The simulation code [14] had been compared with [11] giving excellent results. Other simulation codes are available [15] which are not yet compared with the results presented in this paper.

2. Experimental setup

The tested silicon bent crystals have two different structures. Strip (ST) crystals are bent through the crystalline axis (1 1 0), while the Quasi–Mosaic (QM) crystals are bent through the (1 1 1) crystalline axis. In both cases, anticlastic forces generate the crystal curvature. The difference between ST and QM is in the interplanar potential created by the distance between the planes. The strip crystals have equidistant crystalline planes, so the channels have all the same size, while QM crystals have a ratio 1:3 for subsequent planes.

Ten crystals were selected to perform a complete analysis, and a list with their manufacturing specifications is given in Table 1. The analysis of the crystal STF45 is presented as example; this crystal was tested in 2010. The dimensions of the strip, which correspond to the x, y and z coordinates are $0.3 \times 55 \times 2\ \text{mm}^3$; the bending radius is 13.33 m and the bending angle is about 150 μrad.

A silicon microstrip telescope is used to measure particles trajectories upstream and downstream of the crystal. The telescope and the experimental layout are described in [16]. Five two dimensional silicon detectors with microstrip sensors are arranged to measure at five points the transverse coordinate orthogonal to the beam direction. The microstrips are coupled in pairs orthogonally, for an active area of $3.8 \times 3.8\ \text{cm}^2$. The telescope layout is shown in the Fig. 1. As discussed in [16] the dominant contribution to the angular resolution is due to the multiple scattering of the particles with the sensors, while the position resolution of the impact parameter at the crystal position is influenced by the closest position of the sensor to the goniometer position. The incoming track is reconstructed from an extrapolation of the line reconstructed with the points measured by the first two planes. The outgoing tracks are reconstructed fitting the points measured

* Corresponding author at: INFN Sezione di Roma, Piazzale Aldo Moro 2, 00185 Rome, Italy.

http://dx.doi.org/10.1016/j.nimb.2015.03.001
0168-583X/

Table 1
Crystals manufacturing specifications, provided by PNPI and Ferrara INFN. In the name of the crystal the first two letters give the information on the kind of crystal. In the QM case, x_{CR} and y_{CR} dimensions represent the active area of the crystal.

Crystal	Bending Radius R [m]	Dimension $x_{CR} \times y_{CR} \times z_{CR}$ [mm^3]
STF38	9.00	$1.00 \times 55.0 \times 1.89$
STF45	13.33	$0.30 \times 55.0 \times 2.00$
STF47	68.89	$2.00 \times 55.0 \times 3.10$
STF48	11.75	$1.00 \times 55.0 \times 2.00$
STF49	2.96	$0.50 \times 55.0 \times 0.80$
STF50	11.75	$1.00 \times 55.0 \times 2.00$
STF51	66.67	$2.00 \times 55.0 \times 3.00$
QMP27	15.26	$20.0 \times 40.0 \times 1.77$
QMP29	120.00	$20.0 \times 40.0 \times 6.00$
QMP32	5.48	$20.0 \times 40.0 \times 0.96$

with the last three planes. For a single trajectory, the two tracks upstream and downstream of the crystal, need to have the same impact point at the crystal position. This condition is used as a constraint for the fit. Hence, for each track, three free parameters for each projection on the orthogonal axis are given: the two angles θ_{in} (incoming angle) and θ_{out} (outgoing angle) and the impact point at the crystal position d_0 (impact parameter at $z = 0$). The angular resolution of the telescope is measured in a specific alignment run that is presented in the next section. The resolution is calculated as the angular deflection of the particle ($\Delta\theta = \theta_{in} - \theta_{out}$) when the crystal is not present. The measured resolution is 5.2 μrad for both x and y plane.

2.1. Alignment runs

Alignment runs are performed by measuring the trajectory with the full setup but without the crystal. The key observables are the beam divergence and its profile at the crystal entrance. The main outcome from this analysis is the telescope resolution. This is inferred from the angular distribution $\Delta\theta = \theta_{in} - \theta_{out}$ of the single-track events measured by the telescope without the crystals. In the STF45 case, the beam spot has a double gaussian shape with a transverse sigma of 0.96 mm and 0.72 mm in the horizontal and vertical planes, respectively. The divergence of the beam is found to be 10.67 μrad in x and 7.66 μrad in y. The measured resolution is 5.7 μrad as shown in Fig. 2.

2.2. High statistics runs analysis

The analysis is applied after selecting only the tracks that are impacting on the crystal impact face. Geometrical cuts are performed analyzing the x and y deflection with respect to the x and y impact point of the tracks. The crystal torsion is also corrected: it is estimated on the study of the crystal channeling efficiency as a function of the impact x angle and the vertical impact point.

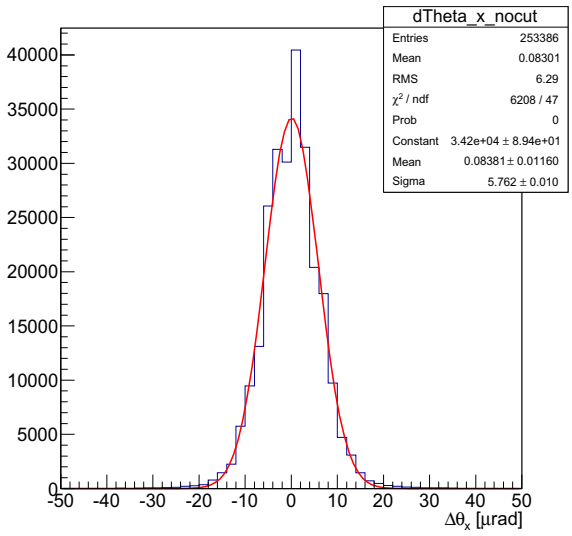

Fig. 2. Run 411: Telescope resolution from the alignment run of the STF45 crystal.

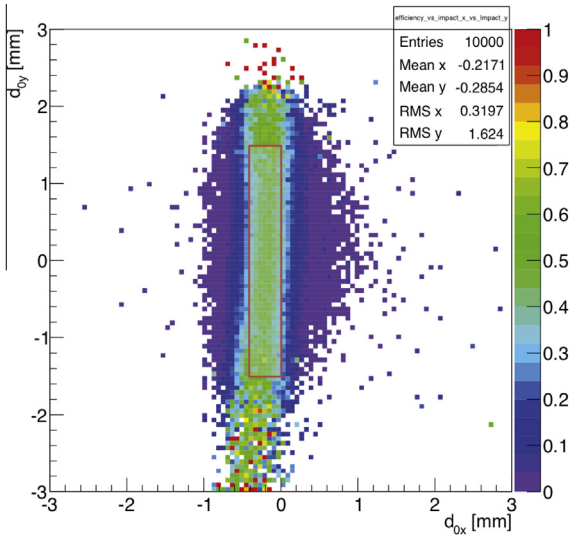

Fig. 3. Channeling efficiency as a function of the impact point on the crystal QMP27 impact face.

3. Analysis details on case study

3.1. Corrections and cuts on data

Three different corrections have to be applied before starting the analysis: geometrical cuts (different for ST and QM crystals), torsion correction, angular cuts. This selection is performed to collect only the tracks of the particles that hit the crystal. Multiple Coulomb scattering is useful to identify these particles. Studying deflection distributions ($\Delta\theta_x$ and $\Delta\theta_y$) as a function of the impact

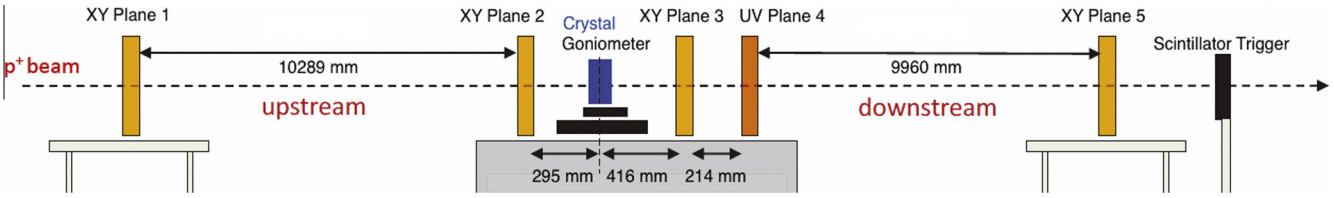

Fig. 1. H8 UA9 Telescope layout. The plane 4 in different color is rotated of 45°. (For interpretation of the references to colour in this figure legend, the reader is referred to the web version of this article.)

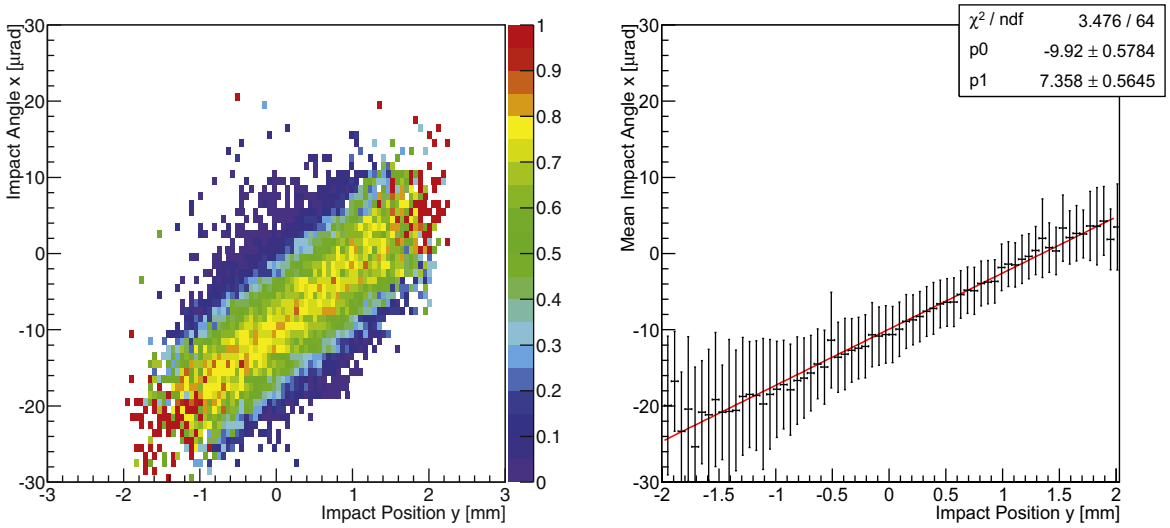

Fig. 4. Left: Channeling efficiency as a function of the x impact angle and the y impact for the STF45 crystal. Right: Mean x impact angle as a function of y impact point, the trend shows the crystal torsion.

point, at the position (d_{0x}, d_{0y}) a larger spread in the gaussian beam profile can be seen. This method is suited for ST crystals while for QM crystals a different selection technique is introduced. A feature of this crystal is an additional bending on the impact face. This bending causes the impact angle relative to the crystalline plane direction to be a function of the impact d_{0x} position. Hence a smaller area of the impact face has to be selected for a proper analysis of the crystal properties. The selection is performed studying the channeling efficiency as a function of the impact point at the crystal face (d_{0x}, d_{0y}). The channeling efficiency is defined as the ratio between the channeled particles and the total number of particles that hit the crystal face in each of the 60×60 μm^2 squares in which the total surface is divided:

$$\eta_{QM}(d_{0x}, d_{0y}) = \frac{N_{ch}(d_{0x} + dx, d_{0y} + dy)}{N(d_{0x} + dx, d_{0y} + dy)}. \quad (1)$$

Fig. 3 shows how the selection is performed on an area which has the largest and the most constant value of channeling efficiency.

3.2. Torsion analysis and correction

The torque imposed by the holder is not symmetric hence a torsion in the vertical direction is induced. This effect makes the impact angle relative to the crystalline plane a function of the impact vertical position. An analysis of the channeling efficiency as a function of vertical impact position and horizontal impact angle allows correcting artifacts from torsion. We define it as a function of the x impact angle and the y impact position, as shown in Fig. 4, Left:

$$\eta_{tor}(d_{0y}, \theta_x^{in}) = \frac{N_{ch}(d_{0y} + dy, \theta_x^{in} + d\theta_x^{in})}{N(d_{0y} + dy, \theta_x^{in} + d\theta_x^{in})}. \quad (2)$$

The steps $\delta z = 0.06$ mm and $\delta\theta_x^{in} = 1$ μrad are given by the apparatus resolution. From Fig. 4, Left a measurement of the torsion can be made, as well as a definition of the x impact angle relative to the cristalline planes. The mean x impact angle as a function of the d_{0y} is calculated and the plot is shown in Fig. 4, Right. A linear fit of these data (Fig. 4, Right) gives the torsion value and the offset angle with respect to crystalline planes. In this example $t = 7.36$ μrad/mm, with an offset of -9.92 μrad.

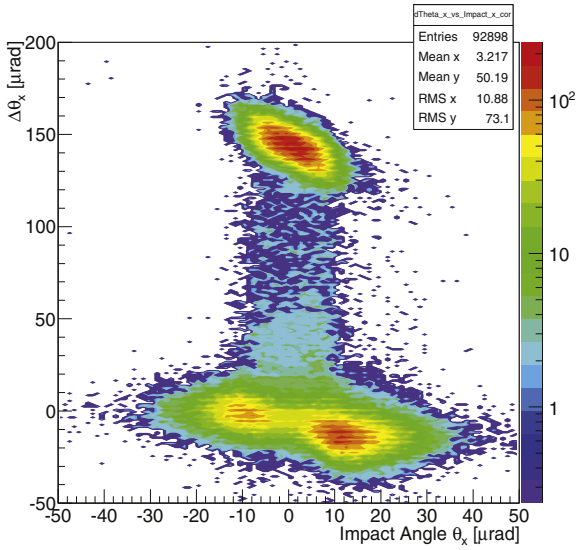

Fig. 5. Run 415. The x deflection angle vs. the x impact angle at the crystal surface.

Correcting the impact angle as in Eq. (3) the impact angle relative the crystalline planes for all the particles that hit the crystal is obtained:

$$\theta_x^{corr} = \theta_x^{rel} - (t \cdot d_{0y} + \Theta_{rel}^{off}). \quad (3)$$

After geometrical cuts and the torsion correction, a 2D plot with x deflection as a function of x impact angle is produced as shown in Fig. 5.

After this correction, one can perform the angular cuts to select only the particles impacting on the crystal with an impact angle equal or smaller than the critical channeling angle. This solution is applied in order to define the channeling efficiency as a function of the particles undergoing channeling. The critical angle for 400 GeV protons in a silicon crystal is ~ 10 μrad, hence the angular cuts are ± 5.0 μrad and ± 10.0 μrad. The gaussian fit on the channeling peak gives the bending angle of the crystal.

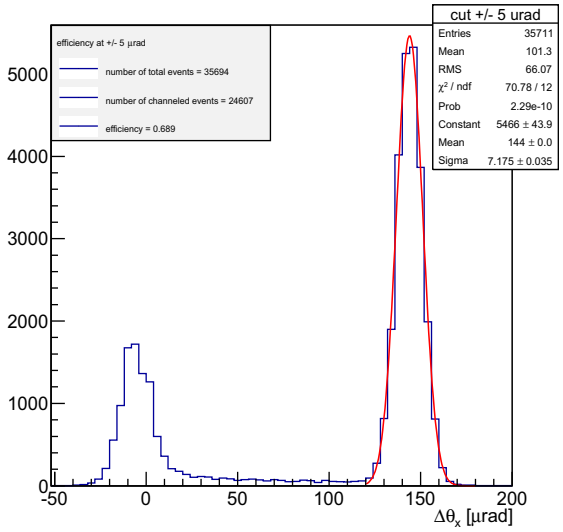

Fig. 6. Run 415. The deflection in the *x* direction withan angular cut of ±5.0 µrad; the value of the efficiency is reported in the insert.

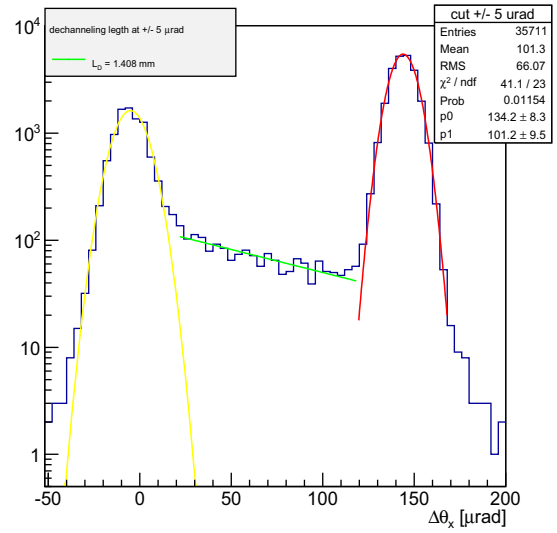

Fig. 7. Run 415. Dechanneling length using a ±5.0 µrad angular cut.

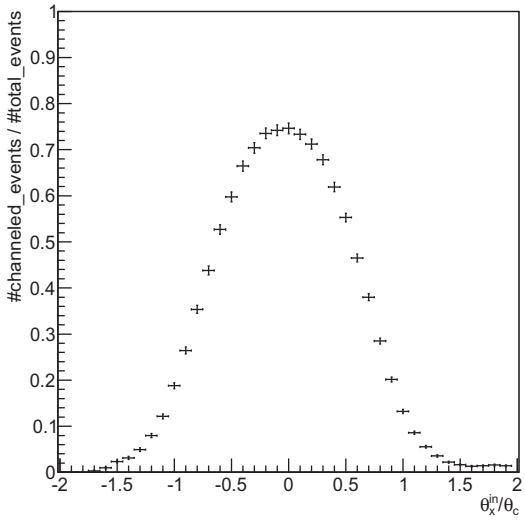

Fig. 8. Run 415. Channeling population, normalized to the number of total particles, as a function of the *x* impact angle, normalized to the critical channeling angle.

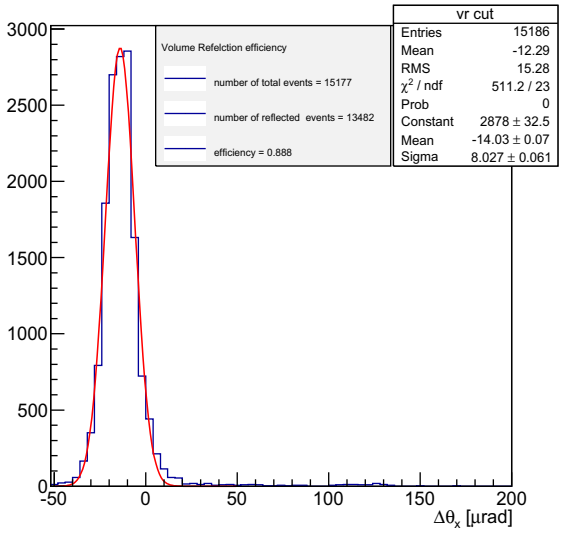

Fig. 9. Run 415. Channeling population, normalized to the number of total particles, as a function of the *x* impact angle, normalized to the critical channeling angle.

3.2.1. Channeling efficiency

The channeling efficiency is calculated as the ratio between the number of channeled particle and the total number of particles impinging on the crystal within a given angular range. Typically two different cuts of ±5.0 µrad and of ±10.0 µrad are considered. The particles in channeling are calculated as the ones within $\pm 3\sigma$ of the channeling peak, as shown in Fig. 6. In this example a channeling efficiency of 0.69 is measured. An efficiency of 0.53 is calculated for particles when ±10.0 µrad cut is used.

3.2.2. Nuclear dechanneling length

Nuclear dechanneling length is an effect that is predominant in short bent crystal, and is described in [17]. The relative dechanneling length (l_d) is also calculated for two angular cuts of ±5.0 µrad and ±10.0 µrad. An exponential fit is performed between $+3\sigma$ from the mean value of the amorphous peak and -3σ from the mean value of the channeling peak, as shown in Fig. 7. The dechanneling length is measured to be 1.41 ± 0.14mm and 1.28 ± 0.09mm for the angular cut of ±5.0 µrad and ±10.0 µrad, respectively.

Table 2
Summary of the crystal characteristics measured in the analysis.

Crystal	Bending angle θ_b^{meas} [µrad]	Length z_{CR} [mm]	Torsion t [µrad/mm]
STF38	211.23 ± 0.05	1.89	−5.55 ± 0.41
STF45	143.78 ± 0.07	2.00	7.36 ± 0.57
STF47	34.10 ± 0.02	3.10	−2.52 ± 0.29
STF48	143.60 ± 0.02	2.00	6.94 ± 0.33
STF49	246.65 ± 0.03	0.80	5.31 ± 0.31
STF50	139.59 ± 0.01	2.00	4.99 ± 0.37
STF51	33.40 ± 0.01	3.00	−1.08 ± 0.25
QMP27	108.13 ± 0.01	1.77	1.38 ± 0.50
QMP29	33.95 ± 0.01	6.00	−0.22 ± 0.25
QMP32	170.69 ± 0.05	0.96	−0.65 ± 0.58

3.2.3. Population analysis

An analysis on the channeling, dechanneling and transition region (from amorphous to volume reflection) and is performed as a function of the *x* impact angle. The analysis is performed using

Table 3
Summary of the channeling efficiency, dechanneling length, for each crystal. In the crystal STF47, STF51 and QMP29 cases, their feature do not allow the analysis in the dechanneling region; the low bending angle do not permit the decoupling of transition region and channeling peak.

Crystal	Channeling $\eta_{ch}^{\theta_c/2}$ [%]	Efficiency $\eta_{ch}^{\theta_c}$ [%]	Dechanneling $L_D^{\theta_c/2}$ [mm]	Length $L_D^{\theta_c}$ [mm]
STF38	48.7 ± 0.5	32.9 ± 0.3	1.11 ± 0.08	0.84 ± 0.04
STF45	68.9 ± 0.5	54.0 ± 0.3	1.41 ± 0.14	1.28 ± 0.09
STF47	52.8 ± 0.2	45.1 ± 0.2	–	–
STF48	52.9 ± 0.1	41.0 ± 0.1	1.71 ± 0.14	1.47 ± 0.08
STF49	46.0 ± 0.4	34.6 ± 0.3	0.19 ± 0.01	0.18 ± 0.01
STF50	54.7 ± 0.1	45.2 ± 0.1	1.52 ± 0.07	1.29 ± 0.08
STF51	48.7 ± 0.1	44.1 ± 0.1	–	–
QMP27	58.6 ± 0.2	50.4 ± 0.2	1.48 ± 0.12	1.35 ± 0.08
QMP29	64.5 ± 0.1	56.2 ± 0.1	–	–
QMP32	50.7 ± 0.8	40.9 ± 0.5	0.46 ± 0.05	0.37 ± 0.04

Table 4
Summary of the volume reflection angle and efficiency, measured in the range $[2\theta_c,3\theta_c]$. In the crystal STF47 case, its feature do not allow the analysis in the volume reflection region; the low bending angle do not permit the decoupling of volume reflection and amorphous peak.

Crystal	Volume reflection	
	Angle θ_{vr}^{meas} [μrad]	Efficiency $\eta_{vr}^{[2\theta_c,3\theta_c]}$ [%]
STF38	-13.10 ± 0.01	79.3 ± 0.8
STF45	-14.03 ± 0.12	88.8 ± 0.3
STF47	–	–
STF48	-14.15 ± 0.05	76.8 ± 1.3
STF49	-9.14 ± 0.23	91.9 ± 1.5
STF50	-13.57 ± 0.03	76.0 ± 0.2
STF51	-14.41 ± 0.02	79.4 ± 0.5
QMP27	-12.85 ± 0.06	90.5 ± 1.5
QMP29	-13.82 ± 0.04	86.8 ± 1.1
QMP32	-11.21 ± 0.32	88.2 ± 2.3

a floating bin technique showing the channeling efficiency as a function of the x impact angle. An analysis of the channeling region is performed as shown in Fig. 8. The channeled efficiency has a maximum value for $\theta_x^{in} = 0$.

3.2.4. Volume reflection analysis

The volume reflection effect is analyzed in the region between $+2\theta_c$ and $+3\theta_c$. Those value are chosen to be independent form the crystals characteristic. For the case study the volume reflection bending angle is found to be -14.03 ± 0.12 μrad, as shown in Fig. 9. The calculation of volume reflection efficiency is performed similarly to channeling efficiency calculation. For STF45 the volume reflection efficiency is 0.89.

4. Summary of all crystals

A summary of the measurements made in this analysis is reported in the following tables. Table 2 summarizes the bending angle measured in the analysis, from the gaussian fit of the channeling peak, and the torsion for each crystal. In Table 3, the efficiency and dechanneling length values are reported for all the crystals. Volume reflection analysis is summarized in Table 4 reporting reflection angle and efficiency.

5. Conclusions

The crystal characterization with extracted proton beams is useful to check the crystal and to compare the results with crystal simulation routines. For the first time all the data collected from 2010 to 2012 have been processed consistently; this allowed to identify 10 crystals of interest for which different analysis routines were developed.

The performed analysis has produced the following results: channeling efficiency for single proton pass (with coherent angular cut), nuclear dechanneling length, population of particles in the different effect regions, mean gaussian value in the channeling and transition region.

The main result is the statically complete analysis on the different effects of the interaction of protons with bent silicon crystals. This represents a starting point for the comparison between the different crystal simulation routines. Other measurements, such as the dechanneling population and the volume capture length, are new results and would be the subject of a future publication. The validation of the simulation routines is ongoing. It represents a crucial step for a predictive analysis of crystal collimation in high intensity operation of hadron colliders, such as the HL-LHC.

Acknowledgments

A thanks goes to everyone involved in the useful discussion and data taking leading to these results. In particular the whole UA9 Collaboration (especially the INFN Rome group) and the LHC Collimation Team in the CERN BE/ABP group.

References

[1] J. Stark, Phys. Z. 13 (1912) 973.
[2] J. Lindhard, K. Dan, Viddensk. Selsk. Mat. Phys. Medd. 34 (1) (1965).
[3] V.M. Biryukov, Y.A. Chesnokov, V.I. Kotov, Crystal Channeling and its Application at High Energy Accelerators, Springer, 1996.
[4] D. Mirarchi et al., Final layout and expected cleaning for the first crystal-assisted collimation test at the LHC, in: IPAC2014-MOPRI110.
[5] W. Scandale et al., First results on the SPS beam collimation with bent crystals, Phys. Lett. B 692 (2010) 78.
[6] W. Scandale et al., Comparative results on collimation of the sps beam of protons and Pb ions with bent crystals, Phys. Lett. B 703 (2011) 547–551.
[7] W. Scandale et al., Strong reduction of the off-momentum halo in crystal assisted collimation of the SPS beam, Phys. Lett. B 714 (2012) 231–236.
[8] W. Scandale et al., Optimization of the crystal assisted collimation of the SPS beam, Phys. Lett. B 726 (2013) 182–186.
[9] Available at: <http://www.lnf.infn.it/conference/channeling2014/home.php>.
[10] Available at: <http://lhc-collimation-upgrade-spec.web.cern.ch/LHC-Collimation-Upgrade-Spec/H8input.php>.
[11] D. Mirarchi et al., A crystal routine for collimation studies in circular proton accelerators, Nucl. Instr. Meth. B (submitted for publication).
[12] E. Bagli et al., A model for the interaction of high-energy particles in straight and bent crystals implemented in Geant4, Nucl. Instr. Meth. B (submitted for publication).
[13] P. Schoofs et al., Recent advances in the FLUKA event generator for crystal channeling, Nucl. Instr. Meth. B (submitted for publication)
[14] A.M. Taratin, Particle channeling in a bent crystal, Phys. Part. Nucl. 29 (1998) 437–462.
[15] A. Babaev, S.B. Dabagov, Simulations of planar channeling of relativistic nuclei in a bent crystal, Eur. Phys. J. Plus 127 (2012) 62.
[16] M. Pesaresi et al., Design and performance of a high rate, high angular resolution beam telescope used for crystal channeling studies, JINST 6 (2011) P040006.
[17] W. Scandale et al., Observation of nuclear dechanneling for high-energy protons in crystals, Phys. Lett. B 680 (2009) 129–132.